Journal of Photochemistry and Photobiology A: Chemistry 205 (2009) 145–150

Contents lists available at ScienceDirect

Journal of Photochemistry and Photobiology A: Chemistry

journal homepage: www.elsevier.com/locate/jphotochem

Luminescence based on energy transfer in silica doped with lanthanide titania ($Gd_2Ti_2O_7$:Ln^{3+}) [Ln^{3+} = Eu^{3+} or Dy^{3+}]

M. Saif*

Department of Chemistry, Faculty of Education, Ain Shams University, Roxy, 11711 Cairo, Egypt

ARTICLE INFO

Article history:
Received 30 January 2009
Received in revised form 22 April 2009
Accepted 24 April 2009
Available online 3 May 2009

Keywords:
Luminescence
Silica
Lanthanide ions
Gadolinium titanate

ABSTRACT

Gadolinium titanate doped with lanthanide metal ions ($Gd_2Ti_2O_7$:Eu^{3+} or Dy^{3+}) and embedded in silica matrix is prepared by sol–gel process. TG/DSC, IR, Raman spectroscopy and TEM have been used to investigate thermal, structural and optical properties of xerogels annealed at 1100 °C. The photoluminescence (PL) spectra showed the characteristic emission bands of Eu^{3+} and Dy^{3+} in the host matrix. A significant increase in the PL lifetime is observed in the silica nanocomposite matrix relative to the pure europium-doped gadolinium titanate nanoparticles at the same dopant concentration. The effects of lanthanide metal ion concentration and thermal treatment on the luminescence properties of Ln^{3+} ion are investigated.

1. Introduction

In the last decades, much research has been focused on luminescent materials containing trivalent lanthanide ions, Ln^{3+} [1,2]. Rare earth compounds have been widely used in high performance luminescent devices, magnets, catalysts, and other functional materials owing to the numerous well defined transition modes involving 4f shell of their ions [3]. The photoluminescent properties of Eu^{3+} and Dy^{3+} ions make them other potential candidates for use in luminescent materials [2].

Amorphous oxide materials doped with inorganic lanthanide luminescent material are candidates for optical photonic applications including solid-state lasers, optical waveguides, fiber amplifiers and phosphors [4]. The outstanding mechanical, thermal and optical properties of silica amorphous materials make them especially attractive matrices for luminescent Ln^{3+} ions [4].

Pyrochlore oxides of general formula $Ln_2A_2O_7$ have emerged as important functional materials due to their interesting thermal, electrical, optical, magnetic and catalytic properties [5]. They are of great interest to a wide community of materials scientists not only because of the fascinating phenomena and properties exhibited, but also due to their potential technological applications in fuel cells and other similar devices [6].

The pyrochlore rare earth (Ln) oxides ($Ln_2A_2O_7$, A = Ti, Sn, Zr, Hf) have a face centered cubic crystal structure, in which Ln^{3+} and transition-metal A^{4+} ions locate on the sites 16d and 16c, respectively [7]. Although a wide range of pyrochlore-type dititanate compounds ($Ln_2Ti_2O_7$) have been synthesized and studied from a structural, magnetic and electrical point of view from [8–13], only a few have been attempted in explaining the PL properties of Ln^{3+} ions doped in dititanate ceramics [7]. On the other hand, the visible emissions of Eu^{3+}, in the red region, are particularly interesting for polychromatic displays and imaging. Additionally, for Eu^{3+} ions, a given optical center in different host lattice will exhibit different optical properties due to changes of the surroundings of the center [7]. Moreover, dysprosium ion has been recognized as one of the most efficient lanthanide (Ln^{3+}) ions for obtaining visible and mid-infrared emissions. Dysprosium doped in different matrices such as glasses and bromide phosphor is now attracting a practical interest and can be utilized for the optical amplification in telecommunication systems and a visible solid-state laser [14].

Pyrochlore dititanate compounds are prepared using several methods such as liquid mix technique, solid-state reaction, mechanical milling and sol–gel method [8,9,15,16]. In the past years, sol–gel process has taken wide popularity. It offers new approaches to the synthesis of homogeneous materials with desirable properties of hardness, optical transparency, chemical durability, tailored porosity, and thermal resistance [1]. However, the characteristics and properties of a particular sol–gel inorganic network are related to a number of factors that affect the rate of hydrolysis and condensation reactions, such as pH, temperature and time of reaction, reagent concentrations, catalyst nature and concentration, aging time and temperature and drying. By controlling these factors, it is possible to vary the structure and properties of the sol–gel derived inorganic network over wide ranges. In comparison with traditional method, sol–gel method offers a better chemical homo-

* Tel.: +(02010) 9642295; fax: +(02) 22581243.
E-mail address: mona_saif1@yahoo.com.

1010-6030/$ – see front matter © 2009 Elsevier B.V. All rights reserved.
doi:10.1016/j.jphotochem.2009.04.020

geneity and low-temperature processing. It also allows the control of the chemical pore size distribution of the nanoparticulate materials [6]. Moreover, sol–gel method is useful in the preparation of nanocrystallites-doped glasses with relatively high particle concentrations, small particle diameter and uniform size distribution [17].

The present research focuses on the preparation and optical as well as structural characterization of new photoluminescent pyrochlore dititanate nanoparticles [$Gd_2Ti_2O_7$:Eu^{3+} or Dy^{3+}] dispersed in silica matrices.

2. Experimental

2.1. Materials

The starting materials used in these studies are analytical grade. Titanium(IV) isopropoxide, $Ti[O(C_3H_7)]_4$ (TTIP) is purchased from Fluka. Lanthanide(III) salts: $Gd(NO_3)_3{\cdot}6H_2O$, $Dy(NO_3)_3{\cdot}xH_2O$, $EuCl_3{\cdot}6H_2O$ and tetramethoxysilane, $Si(OCH_3)_4$ (TMOS) are obtained from Aldrich. Methanol and hydrochloric acid (Sigma–Aldrich) are also used as received.

2.2. Sample preparation

Pyrochlore dititanate compounds [$Gd_2Ti_2O_7$:Eu^{3+} or Dy^{3+}] nanocomposite in silica matrices and pure lanthanide-doped gadolinium titanate are obtained by sol–gel process. The samples are prepared in the process involving four stages.

The former stage is mixing of gadolinium nitrate (0.250 g), TTIP (0.360 ml), methanol (4.00 ml), water (0.130 ml) together in the presence of few drops of HCl. Then 0.5, 1.0, 2.0, 5.0, 10.0 and 20 mol% of either europium chloride or dysprosium nitrate dopant is added to the above mixture under stirring for 2 h at room temperature (0.5 mol gadolinium nitrate:1.0 mol TTIP). The second stage, TMOS (2.50 ml) is added to methanol (4.50 ml) and H_2O (0.180 ml) in molar ratio 1.0:10:4.0. Hydrochloric acid (0.020 ml) is added as a catalyst. The solution is vigorously stirred for 4 h. In the third stage, the TMOS and gadolinium titanate solutions are mixed together and stirred for 12 h at room temperature. Finally, highly transparent sols are obtained after stirring, which aged for 24 h till the formation of gel. The gel is dried at 70 °C. The powder is calcined at two different temperatures (800 and 1100 °C) for 8 h.

In the meantime, pure $Gd_2Ti_2O_7$ doped with 5.0 mol% of Eu^{3+} or 1.0 mol% Dy^{3+} is also prepared in the same way without any addition of TMOS.

The following labels are used throughout the text: GTE:$Gd_2Ti_2O_7$:Eu^{3+} nanoparticle sample with 5.0 mol% of Eu^{3+} ion; GTD:$Gd_2Ti_2O_7$:Dy^{3+} nanoparticle sample with 1.0 mol% of Dy^{3+} ion; GTES and GTDS refer to $Gd_2Ti_2O_7$:*x* mol% Eu^{3+} and $Gd_2Ti_2O_7$:*x* mol% Dy^{3+} embedded in silica matrices, respectively.

2.3. Characterization methods

The prepared samples are characterized in a number of ways. Transmission electron microscopy (TEM) is measured using a Jeol model JEM-1230 TEM operated at 100 kV. X-ray diffraction (XRD) analysis is made using a D/max γA X-ray diffractometer (X'Pert Pro, Japan) with Cu Kα radiation (Kα = 0.15418 nm) at 45 kV and 40 mA. FTIR spectra of the surface of the samples are recorded using a Nicolet Magna IR 760. Raman scattering spectra are recorded with a Horiba Jobin Yvon Raman spectrometer, using the 632.817 nm He–Ne laser for excitation. The light beam is focused through a standard Olympus microscope with a 100× lens down to 5–10 μm in diameter. Differential scanning calorimetry (DSC) and thermogravimetry analyses (TGA) are performed using a PerkinElmer PYRIS TGA, under N_2 gas, at a heating rate of 10 °C/min. The temperature ranged from room temperature to 800 °C in order to obtain crystallization and phase-transformation data. The photoluminescence and lifetime data of the prepared samples are obtained using a Photon Technology International (PTI QM) spectrofluorometer. The PL lifetime data analysis is obtained using PTI's software, FeliX32™.

3. Results and discussion

3.1. Thermal analysis

DSC and TG curves for $Gd_2Ti_2O_7$:Eu^{3+} or Dy^{3+} nanoparticles embedded in silica matrices (GTES and GTDS (5.0 mol% of Eu^{3+} ion and 1.0 mol% of Dy^{3+})) are given in Fig. 1(a and b). Two stages of weight loss within the range 25–800 °C occur with an overall weight loss of 23.90 and 26.50% for GTES and GTDS, respectively. The first stage for both occurs in the temperature range 25–140 °C, and could be assigned to hydrolysis and polycondensation reactions of the unreacted alkoxy groups during the sol–gel process [18–20]. In addition, evaporation of water, which is physically occluded inside the pores of silica matrix, could occur. In the second stage (140–800 °C), the weight loss is attributed to burn out of the organic residue [20].

The DSC scans for the prepared samples exhibit one broad endothermic peak at 140 °C, which can be attributed the dehydroxylation process of surface-attached H_2O and OH groups [18].

3.2. Structure and morphology

Fig. 2(a–d) presents XRD patterns of the pure $Gd_2Ti_2O_7$:Eu^{3+} or Dy^{3+} nanoparticles and embedded in silica matrices (GTE, GTD, GTES and GTDS (5.0 mol% of Eu^{3+} ion and 1.0 mol% of Dy^{3+})) fired at 1100 °C for 8 h in air. The XRD peaks at $2\theta = 14.9$ (1 1 1), 30.4 (2 2 2), 35.2 (4 0 0) and 38.5 (3 3 1) in the spectrum of pure nanoparticle (GTE and GTD samples) are reflection of cubic $Gd_2Ti_2O_7$ phase (JCPDS Card 23-259) (Fig. 2(a and b)) [10,17,21]. The XRD patterns for GTES and GTDS samples in Fig. 2(c and d) show a broad peak between 20.0 and 38.0 (2θ) due to amorphous silica [22]. In addition, gadolinium titanate $Gd_2Ti_2O_7$ diffraction peak ($2\theta = 30.4$) is observed. This indicates that the $Gd_2Ti_2O_7$:Eu^{3+} or Dy^{3+} nanoparticles are highly dispersed in the silica matrix [23]. The average crystal size of the prepared samples calculated from the full width at half maximum (FWHM) of the diffraction peaks using the Scherrer formula [23] are found to be in the range of 7–12 nm.

Fig. 3 shows a representative TEM image of the $Gd_2Ti_2O_7$:Eu^{3+} or Dy^{3+} nanoparticles embedded in silica matrices (GTES and GTDS (5.0 mol% of Eu^{3+} ion and 1.0 mol% of Dy^{3+})). The micrographs for GTES and GTDS in general are typical with crystallites appearing as dark spheres in white silica background [10,23].

3.3. Optical properties

Raman spectra of the pure $Gd_2Ti_2O_7$:Eu^{3+} nanoparticles and embedded in silica matrices (GTE and GTES (5.0 mol% of Eu^{3+} ion)) calcinated at 1100 °C are depicted in Fig. 4. All Raman peaks of the pure nanoparticles are assigned to the cubic $Gd_2Ti_2O_7$ phase of space group *Fd*3*m* (Fig. 4a) [16,17]. The lowest frequency lines, 110 and 214 cm^{-1} are assigned to the F_{2g} mode. The strongest band centered at 306 cm^{-1} is attributed to O–Gd–O bending mode and, in fact, it consists of two modes (E_g, F_{2g}) with very similar frequencies. The band at 450 cm^{-1} is assigned to the Ti–O stretching vibration. Another intense band observed at about 518 cm^{-1} is the A_{1g} mode, which is attributed to Gd–O stretching [16,17]. Raman spectrum of $Gd_2Ti_2O_7$:5.0 mol% Eu^{3+} embedded in silica matrix shows amorphous structure (Fig. 4b). This is due to highly dispersion of the nanoparticles in the silica matrix. Similar behavior occurred with

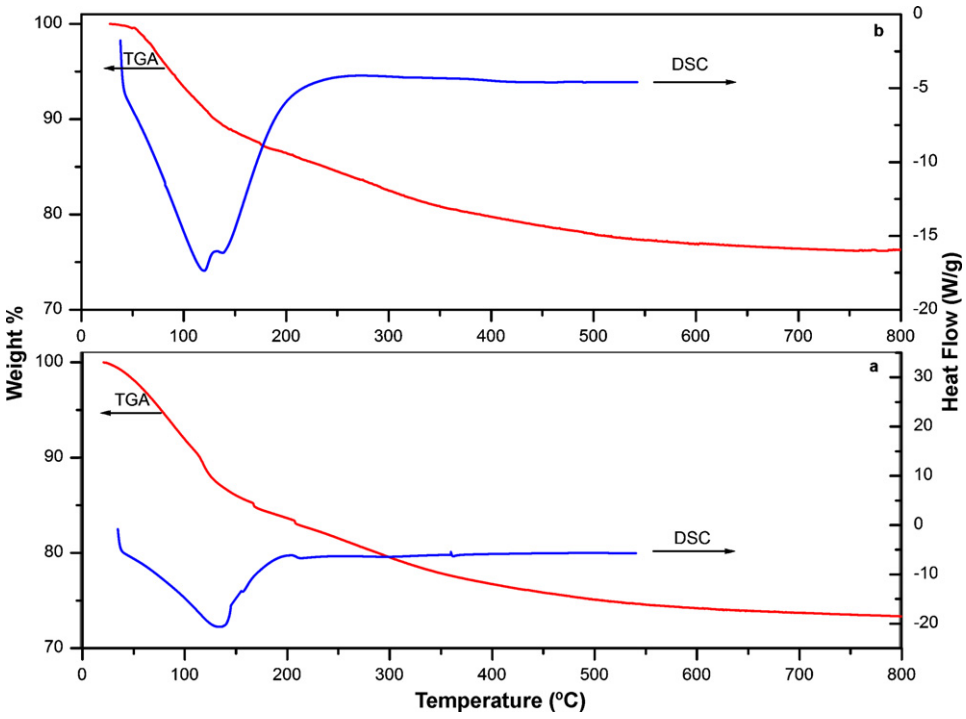

Fig. 1. TGA/DSC curves of (a) EGTS and (b) DGTS samples.

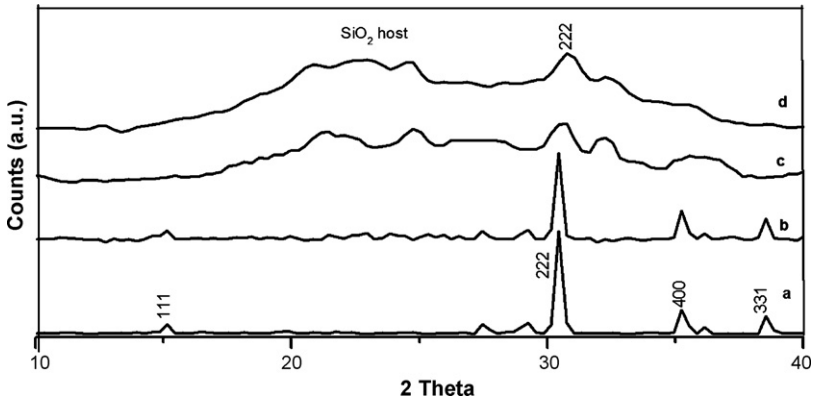

Fig. 2. XRD patterns for as-prepared samples of (a) GTE, (b) GTD, (c) GTES and (d) GTDS calcinated at 1100 °C for 8 h.

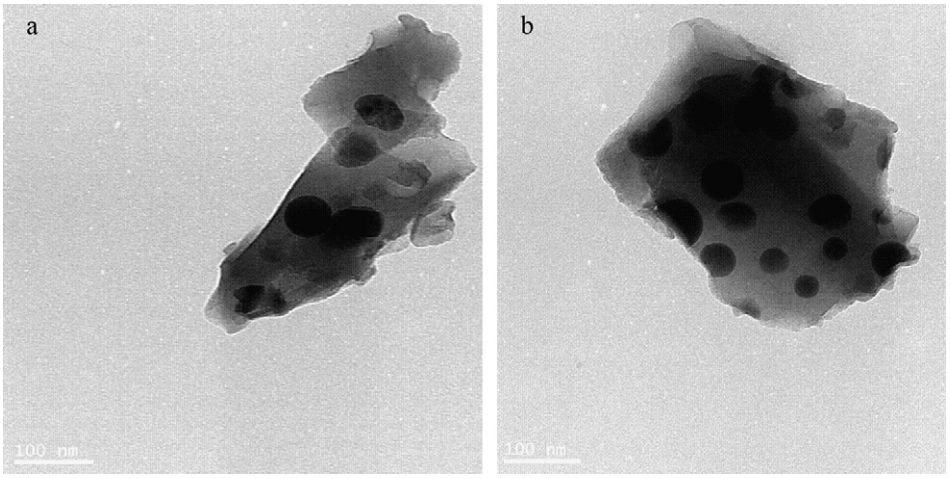

Fig. 3. TEM images of (a) GTES and (b) GTDS calcinated at 1100 °C for 8 h.

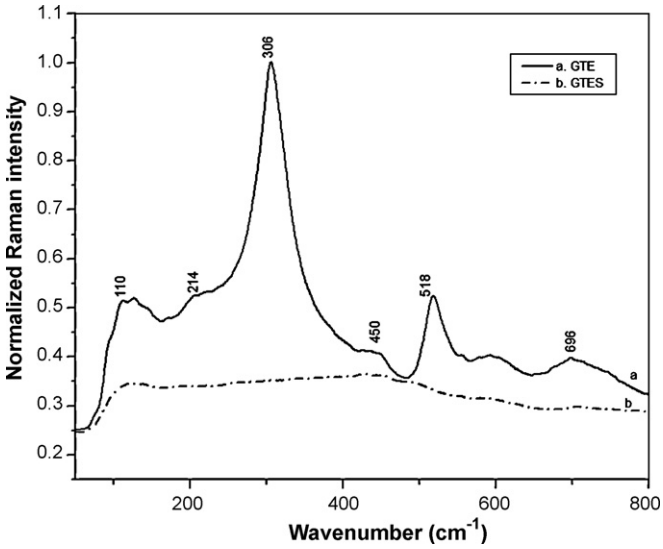

Fig. 4. Raman spectra of (a) GTE and (b) GTES samples calcinated at 1100 °C for 8 h.

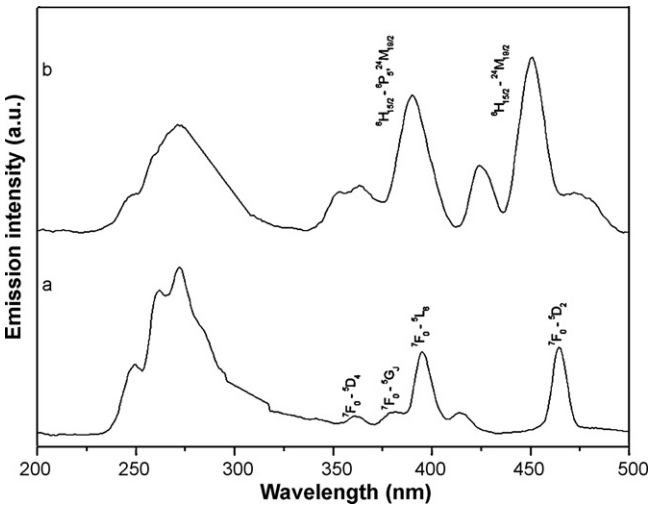

Fig. 5. The excitation spectra of (a) GTES (λ_{em} = 614 nm) and (b) GTDS (λ_{em} = 571 nm).

pure $Gd_2Ti_2O_7$:Dy^{3+} and embedded nanoparticle in silica matrix (GTD and GTDS (1.0 mol% of Dy^{3+} ion)), respectively.

Table 1 lists the main bands and their assignments of the IR spectra of pure $Gd_2Ti_2O_7$:Eu^{3+} or Dy^{3+} nanoparticles and embedded in silica matrices (GTE, GTD, GTES and GTDS (5.0 mol% of Eu^{3+} ion and 1.0 mol% of Dy^{3+})). The FT-IR spectra of pure $Gd_2Ti_2O_7$:Eu^{3+} or Dy^{3+} nanoparticles (GTE and GTD) contain two bands at 667 and 552 cm^{-1}. These bands are attributed to Ti–O stretching vibrations in the TiO_6 octahedron and Gd–O stretching vibration frequency in the tetrahedron of pyrochlore, respectively [17,18]. In addition, these samples exhibit small broad band centered at 449 cm^{-1} characteristic of the Ti–O–Ti vibration [18].

FT-IR spectra of $Gd_2Ti_2O_7$:Eu^{3+} or Dy^{3+} nanoparticles embedded in silica matrices (GTDS and GTES) show bands at 1070 and 457 cm^{-1}. These two bands are related to the stretching of the Si–O–Si and bending of the O–Si–O vibrations [24]. Also, weak features are observed at 1630 and 3400 cm^{-1}, due to OH bending and stretching modes of adsorbed water, respectively [25].

The excitation spectra of $Gd_2Ti_2O_7$:Eu^{3+} and $Gd_2Ti_2O_7$:Dy^{3+} nanoparticles embedded in silica matrices (GTDS and GTES) are collected in Fig. 5(a and b). The intense broad band observed in the range between 230 and 336 nm is attributed to the $Gd_2Ti_2O_7$ host excitation band [7,10]. Other excitation bands in the range 350–500 nm are ascribed to $4f^n$–$4f^n$ transitions in the lanthanide ions (Eu^{3+} and Dy^{3+}) [23].

The PL spectra of the $Gd_2Ti_2O_7$:Eu^{3+} nanoparticles and embedded in silica matrix (GTE and GTES (5.0 mol% Eu^{3+})) have been measured after excitation at 270 nm and are presented in Fig. 6a. The emission spectra show the characteristic red luminescence of the trivalent europium ion. The bands at 575, 590, 614, 652 and 694 nm are corresponding to $^5D_0 \rightarrow {}^7F_0$, $^5D_0 \rightarrow {}^7F_1$, $^5D_0 \rightarrow {}^7F_2$, $^5D_0 \rightarrow {}^7F_3$ and $^5D_0 \rightarrow {}^7F_4$ transitions.

The $Gd_2Ti_2O_7$ adopts a pyrochlore structure, which is an anion-deficient derivative of fluorite with Gd^{3+} ions locate in octahedral sites [7]. The doped Ln^{3+} occupies the Gd^{3+} site based on their close ionic radius and the same valence state in $Gd_2Ti_2O_7$, without changing the original inversion symmetry. It is expected that the magnetic dipole transition ($^5D_0$–$^7F_1$) of Eu^{3+} dominates in the emission spectrum and all other transitions are forbidden [7,23]. Co-existence of both electric ($^5D_0 \rightarrow {}^7F_2$) and magnetic dipole ($^5D_0 \rightarrow {}^7F_1$) allowed transitions from the samples in our study is because of the significant lattice distortion brought about by higher concentration of Eu^{3+} incorporation. Further, due to the same reason significant number of Eu^{3+} ions will be present on the surface of the nanoparticles and the emission spectrum is dominated by surface Eu^{3+} ions, which has got highly distorted environment [23].

It is well known that the PL intensity ratio of $^5D_0$–$^7F_2$ to $^5D_0$–$^7F_1$, called as asymmetry ratio [7], gives a measure of the degree of distortion from inversion symmetry of the local environment around the Eu^{3+} ions in the host matrix. From the emission spectra of pure and embedded in silica samples (GTE and GTES (5.0 mol% Eu^{3+})) after 270 nm excitation, the asymmetric ratio of luminescence has been calculated to be 1.3 and 2.4, respectively. The increase in asymmetric ratio for nanoparticles dispersed in silica in comparison with pure nanoparticle is explained due to the fact that Eu^{3+} ions on the surface of the $Gd_2Ti_2O_7$:Eu^{3+} nanoparticles feel a more distorted environment brought about by the presence of both gadolinium titanate and silicon structural units present around them. This gives rise to an increase in intensity of the electric dipole allowed $^5D_0$–$^7F_2$ transition, resulting in an increase in the asymmetric ratio [23,26–28].

Moreover, dispersion of europium-doped gadolinium titanate nanoparticles in silica matrix enhances the probability of energy transfer process, which is confirmed by the increase of the lifetime of the excited state of Eu^{3+} ($\iota_{GTE\,(5\%\,Eu^{3+})} = 25.30 \pm 6.00\,\mu s$, $\iota_{GTES(5\%\,Eu^{3+})} = 1209 \pm 128\,\mu s$). This might be due to the effective shielding of surface Ln^{3+} ions in $Gd_2Ti_2O_7$ nanoparticles from the adsorbed water molecules by silica matrix [4].

PL spectrum of $Gd_2Ti_2O_7$:Dy^{3+} nanoparticles embedded in silica matrix (GTDS (1.0 mol% Dy^{3+})) upon excitation with light of 270 nm is shown in Fig. 6b. The sample has two emission bands: one is centered at 485 nm (blue) and another is at 571 nm (yellow). They are assigned to the Dy^{3+} electronic transitions of $^4F_{9/2} \rightarrow {}^6H_{15/2}$ and $^6H_{13/2}$ energy levels, respectively [29]. The main emission [$^4F_{9/2} \rightarrow {}^6H_{13/2}$ (571 nm)] is constituted of symmetrical broad band with a full width at half maximum (FWHM) around 13 nm. This broad emission band is due to highly distorted environment around the rare earth metal ions in that amorphous host material [23,30]. No yellow emission is detected from pure $Gd_2Ti_2O_7$:Dy^{3+} (GTD (1%

Table 1
IR spectral data (cm^{-1}) of the prepared samples.

Compound	Main absorption bands and their assignments (cm^{-1})
GTE and GTD	3400 (ν_{H-O-H}), 1630 (ν_{H-O-H}), 667(ν_{Ti-O}), 552 (ν_{Ti-O}), 449 ($\nu_{Ti-O-Ti}$)
GTES and GTDS	3400 (ν_{H-O-H}), 1630 (ν_{H-O-H}), 1070 ($\nu_{Si-O-Si}$), 960 (ν_{Si-OH}), 800 (ν_{O-Si-O}), 457 (δ_{O-Si-O})

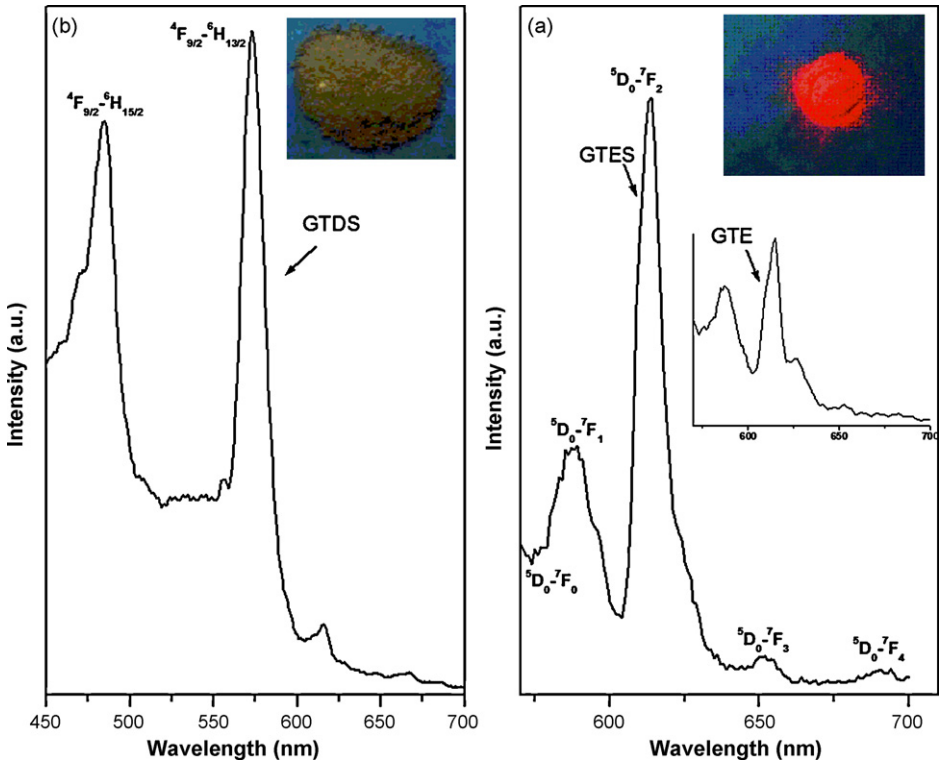

Fig. 6. The emission spectra of (a) GTES, GTE and (b) GTDS at (λ_{ex} = 270 nm). Insets: the emission photographs of the GTES and GTDS samples.

Dy^{3+})) in comparison with $Gd_2Ti_2O_7$:Dy^{3+} nanocomposite at the same concentration of Dy^{3+} (GTDS (1% Dy^{3+})).

Fig. 7 shows the PL decay curves of the $Gd_2Ti_2O_7$:Eu^{3+} and $Gd_2Ti_2O_7$:Dy^{3+} nanoparticles embedded in silica matrices (GTES (5.0 mol% Eu^{3+} and GTDS 1.0 mol% Dy^{3+})) samples. To obtain the optimum dopant concentration, a series of samples doped with different Ln^{3+} concentrations are prepared, and the PL lifetime of $^5D_0$ state of Eu^{3+} and $^4F_{9/2}$ state of Dy^{3+} are measured (Fig. 7 (inset)). It is obvious that the PL lifetime of Eu^{3+} and Dy^{3+} increases with increase of their concentration, until reaching a maximum value, then decreases with increasing their content due to the concentration quenching [3]. Thus, the optimum concentrations for Eu^{3+} and

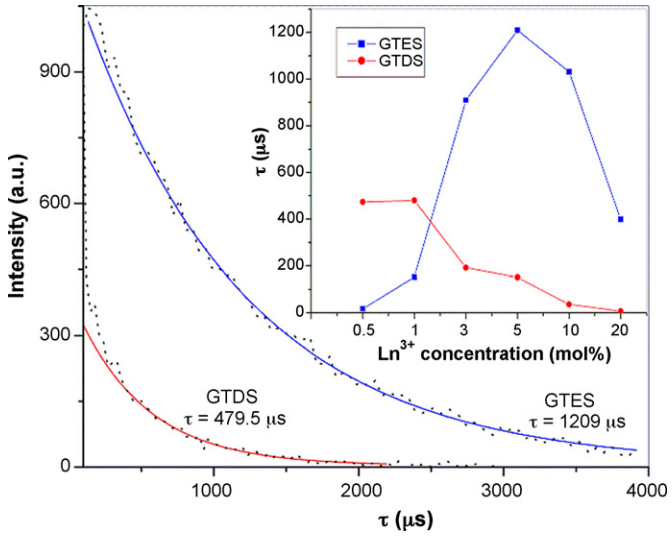

Fig. 7. PL decay curves of GTES and GTDS samples (λ_{ex} = 270 nm). Solid curves represent the best fit of one-exponential decay. Inset: PL lifetime of $^5D_0$ of Eu^{3+} in GTES and $^4F_{9/2}$ of Dy^{3+} in GTDS as a function of Ln^{3+} concentrations.

Table 2
PL lifetime (ι) and fluorescence intensity (I) of 5 mol% Eu^{3+} in GTES and 1 mol% Dy^{3+} in GTDS as a function of annealing temperature.

Anneal temperature (°C)	GTES		GTDS	
	ι (μs)	I (a.u.)	ι (μs)	I (a.u.)
70	15.90 ± 1.6	203.0	11.00 ± 1.6	155.0
800	601.4 ± 121	556.0	56.70 ± 2.9	229.0
1100	1209 ± 128	1196	479.5 ± 17	336.0

Dy^{3+} in the host material are 5.0 mol% (ι = 1209 μs) and 1.0 mol% (ι = 479.5 μs), respectively.

Table 2 shows the effect of thermal treatment on the PL lifetime and luminescence intensity of Eu^{3+} and Dy^{3+} in GTES and GTDS samples (5.0 mol% of Eu^{3+} ion and 1.0 mol% of Dy^{3+}), respectively. It is noted that, with increasing the annealing temperature, the PL intensities of Eu^{3+} and Dy^{3+} are enhanced. This is because with increasing of annealing temperature, the content of impurities in the powder such as OH^-, NO_3^- and residual organic compounds decreases with a consequent increase in the powder crystallinity [10,31]. This observation is confirmed by measuring the PL lifetime of $^5D_0$ of Eu^{3+} in GTES and $^4F_{9/2}$ of Dy^{3+} in GTDS as a function of annealing temperature.

4. Conclusions

In the present study, we successfully prepared new photoluminescent pyrochlore dititanate compounds [$Gd_2Ti_2O_7$:Eu^{3+} or Dy^{3+}] nanocomposite dispersed in silica matrix by sol–gel process. The obtained phosphors $Gd_2Ti_2O_7$:Eu^{3+} or Dy^{3+} nanoparticles dispersed in silica exhibit a red and yellow light emission visible to the naked eye. Moreover, these materials are characterized by amorphous structure and sphere morphology of 7–12 nm particle size. Both lifetimes and PL intensities of GTES and GTDS samples increased with increasing the annealing temperature, and the optimum concentrations for Eu^{3+} and Dy^{3+} in the host material are

determined to be 5.0 and 1.0 mol% of Eu^{3+} and Dy^{3+} in $Gd_2Ti_2O_7$ powder host.

Acknowledgements

I would like to thank Dr. J.T. McLeskey, Jr. Demitry and Everett E. Carpenter, VCU (USA), for lab facilities, and Prof. Dr. M.S.A. Abdel-Mottaleb (Ain Shams University, Egypt) for support, critical discussions and encouragement. Financial support of Egyptian Ministry of Higher Education and Scientific Research is highly appreciated.

References

[1] T. Jüstel, H. Nikol, C. Ronda, Angew. Chem. Int. Ed. 37 (1998) 3084.
[2] M. Zalewska, A.M. Kłonkowski, Opt. Mater. 30 (2008) 725.
[3] W. Di, X. Wang, P. Zhu, B. Chen, J. Solid State Chem. 180 (2007) 467.
[4] A.M. Kłonkowski, M. Zalewska, B. Kościelska, J. Non-Cryst. Solids 352 (2006) 4183.
[5] H. Zhu, D. Jin, L. Zhu, H. Yang, K. Yao, Z. Xi, J. Alloys Compd. 464 (2008) 508.
[6] A. Garbout, S. Bouattour, A.M. Botelho do Rego, A. Ferraria, A.W. Kolsi, J. Cryst. Growth 304 (2007) 374.
[7] Y. Zhang, C. Jia, Z. Su, W. Zhang, J. Alloys Compd. 479 (2009) 381.
[8] S. Yamaguchi, K. Kobayashi, K. Abe, S. Yamazaki, Y. Iguchi, Solid State Ionics 113–115 (1998) 393.
[9] S.A. Kramer, H.L. Tuller, Solid State Ionics 82 (1995) 15.
[10] A.W. Pang, J. Lin, J. Fu, Z.Y. Cheng, Mater. Res. Bull. 39 (2004) 1607.
[11] S.T. Bramwell, M.N. Field, M.J. Harris, I.P. Parkin, J. Phys.: Condens. Matter 12 (2000) 483.
[12] J. Lian, L.M. Wang, R.C. Ewing, L.A. Boatner, Nucl. Instrum. Methods Phys. Res. B 241 (2005) 365.
[13] P.T. Diallo, P. Boutinaud, R. Mahiou, J. Alloys Compd. 341 (2002) 139.
[14] H. Wang, J. Li, G. Jia, Z. You, F. Yang, Y. Wei, Y. Wang, Z. Zhu, X. Lu, C. Tu, J. Lumin. 126 (2007) 452.
[15] S.X. Wang, L.M. Wang, R.C. Ewing, K.V. Govindan Kutty, Nucl. Instrum. Methods Phys. Res. B 169 (2000) 135.
[16] A.F. Fuentes, K. Boulahya, M. Maczka, J. Hanuza, U. Amador, Solid State Sci. 7 (2005) 343.
[17] G. Jose, K.A. Amrutha, T.F. Toney, V. Thomas, C. Joseph, M.A. Ittyachen, N.V. Unnikrishnan, Mater. Chem. Phys. 96 (2006) 381.
[18] A. Garbout, S. Bouattour, M. Ellouze, A.W. Kolsi, J. Alloys Compd. 425 (2006) 88.
[19] W. Hung, S. Fu, J. Tseng, H. Chu, T. Ko, Chemosphere 66 (2007) 2142.
[20] B. Grobelna, J. Alloys Compd. 440 (2007) 265.
[21] K.-M. Lin, C.-C. Lin, C.-Y. Hsiao, Y.-Y. Lia, J. Lumin. 127 (2007) 561.
[22] C. Yang, C. Chen, Appl. Catal. A: Gen. 294 (2005) 40.
[23] R.S. Ningthoujam, V. Sudarsan, S.K. Kulshreshtha, J. Lumin. 127 (2007) 747.
[24] B. Grobelna, M. Szabelski, K. Kledzik, A.M. Kłonkowski, J. Non-Cryst. Solids 353 (2007) 2861.
[25] M. Saif, M.S.A. Abdel-Mottaleb, Inorg. Chim. Acta 360 (2007) 2863.
[26] Q.-M. Wang, B. Yan, Mater. Chem. Phys. 94 (2005) 241.
[27] L. Petit, J. Griffin, N. Carlie, V. Jubera, M. García, F.E. Hernández, K. Richardson, Mater. Lett. 61 (2007) 2879.
[28] B. Yan, X. Su, J. Non-Cryst. Solids 352 (2006) 3275.
[29] X. Liang, C. Zhu, Y. Yang, S. Yuan, G. Chen, J. Lumin. 128 (2008) 1162.
[30] B. Viana, N. Koslova, P. Aschehoug, C. Sanchez, J. Mater. Chem. 5 (1995) 719.
[31] I. Zaręba-Grodzĭ, R. Pązik, W. Tylus, W. Mielcarek, K. Hermanowicz, W. Stręk, K. Maruszewski, Opt. Mater. 29 (2007) 1103.